Microstructure Evolution and Its Effect on Mechanical Properties of Friction Stir Welded AZ80 Magnesium Alloy Joint

Tielong Li [a, b], Lei Cui [a]

[a] *Tianjin Key Laboratory of Advanced Joining Technology, School of Materials Science and Engineering, Tianjin University, Tianjin, 300072, China.*
[b] *Mechanical and Electrical Engineering Department, Yuncheng University, Yuncheng, Shanxi, 044000, China.*

Corresponding author is Lei Cui

Abstract
Friction stir welding (FSW) experiment was conducted on AZ80 extruded sheet. The parameter influence on welding qualities, microstructural evolutions and mechanical properties of the welds were investigated. Main achievements are as follows: defect free welds could be obtained. Optimum parameters are of 1000 rpm rotational speed combined with welding speeds of 80 mm/min and 400 mm/min. Recrystallization and precipitate dissolution would perform at nugget zone (NZ), thermos-mechanically affected zone (TMAZ), and heat affect zone (HAZ). In NZ the β-$Mg_{17}Al_{12}$ precipitates dissolve into the Mg matrix or redistribute along grain boundaries to form net-work like structures. Significant softening behavior was found at NZ, TMAZ, and HAZ. The ultimate tensile strength and elongation of FSW AZ80 welds would reach 289 MPa and 2.6% respectively.
Keywords: FRICTION STIR WELDING, AZ80 MAGNESIUM ALLOY, MICROSTRUCTURES, MECHANICAL PROPERTIES

1. Introduction

AZ80 is a kind of heat precipitate strengthening medium strength magnesium alloy with very good forging capability and acceptable corrosion resistance [1]. Aiming at the need of weight reduction, this very light structure material is being used increasingly for fabricating car wheels, the structure of frame-work of electric vehicle bus, aircraft components[2, 3], etc. For magnesium alloys, conventional arc joining and welding technologies would exhibit a lot of disadvantages of high frequency in forming porosity, large heat affect zone, the loss of alloy elements, and high residual stress [4, 5].

In recent years, it was proposed that as a solid-state welding process, the friction stir welding (FSW) might be a potential joining method in fabricating high quality welds for magnesium alloys by means of its low welding temperatures and no melting and freezing process [6, 7]. As it is reported, many kinds of magnesium alloys like AZ31 [6], AZ61[7], AZ91[8], AE42 [9], and Mg alloys with rare earth element [10] have been successfully welded with FSW. Owing to the thermoplastic process and relatively low heat input of FSW process, sound weld without any welding defect could be easily obtained, but the process window is seemingly narrower than FSW of aluminum alloy [4, 6]. Although works for FSW of magnesium alloys are still very limited, some of the meaningful results could be concluded [11, 12].

The welding quality of magnesium alloy FSW weld is extremely sensitive to the welding parameters. Compare to aluminum alloy the optimum parameter window is somewhat narrow [11]. Cao and Jahazi [6] found that, for FSW of AZ31 2 mm wrought sheets, when the parameter combinations of 2000 rpm rotational speed and welding speed up to 15 mm/s are used, defects of cavity and notch would form inner or at the root of the weld [4]. In FSW magnesium alloy welds, the microstructures in nugget zone (NZ) and thermos-mechanically affected zone (TMAZ) are mainly consist of recrystallized fine grains [13-15]. However, the grain refining extent of weld zone is very limited in such wrought or extruded Mg alloys [6, 16].

Both strength and ductility of Mg-Al alloys are close related to the precipitate which is found as β-$Mg_{17}Al_{12}$ phase with an extremely low melting point of 462°C [17]. So it is believed that not only could recrystallization behavior be observed in the weld zone[18, 19], but also complicated precipitation phase transitions [20]. However, in the current state, to the best of our knowledge, investigations on FSW of AZ80 magnesium alloy have rarely been reported so far.

The main objective of this study is to explore whether high quality welds would be performed with optimum welding parameters, and if so, what characteristics of microstructural evolution could be observed and to what extent the welds' mechanical properties would reach in FSW situations. So, in the present study, we carried out several groups of FSW experiment on 3mm thick AZ80 alloy sheets, and aim at characterizing the microstructure characteristics and exploring the joints mechanical properties.

2. Experimental Details

Commercially AZ80 alloy extruded sheets with the thickness of 3mm were used for carrying out friction stir welding (FSW) experiment. The chemical composition of the alloy by wt% was Al-8.3%, Mn-0.25%, Zn-0.58%, Si-0.02%, and Mg-balance. The basic mechanical properties in the extruded direction were 360MPa in tensile strength, 10.2% in ductility, and 85HV in Vickers hardness. The sheet was first cut into blanks with dimensions of 400×200 mm and then sanded for fabricating butt joints.

The welding experiment was conducted on FSW-RS32-015 FSW welding machine along the extruded direction of the sheet. The welding tool is made of H13 steel and has a 10 mm diameter shoulder and a right threaded 2.85 length taper probe. Details of the tool design are shown in Fig. 1. Three tool rotating speeds of 1000, 1250, and 1500 r/min were selected, and for each rotational speed there are four traverse speeds of 80, 150, 300, and 400 mm/min. Moreover, the heel plunge depth and the tilt angle of the welding tool were uniformly set as 0.15 mm and 2.5°, respectively.

After welding, the weldment was cross-sectioned into some samples for carrying out the macro- and microstructure observations. The sample was ground with water abrasive paper and mechanically polished with magnesia suspension and then etched with oxalic acid for about 25 s. Microscopic observations were then conducted by using OLYMPUS GX51 optical microscopic (OM) and Hatchi-4800 scanning electron microscope (SEM). X-ray diffraction (XRD) was used to investigating the phase composition and transformation of the weld on the basis of previous microstructure observations. With the OM examination had finished, the Vickers hardness values of the weld different regions were conducted along the center line of throat depth test using 432SVD Vickers hardness tester.

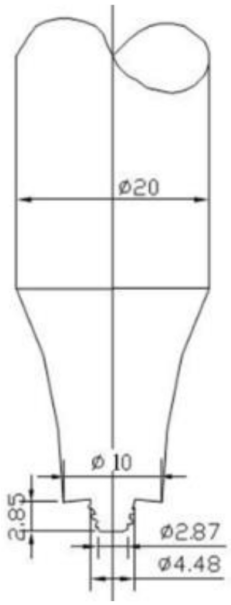

Figure 1. Geometry details of the welding tool

To evaluate the quality of the weld, tensile specimens were sectioned from the obtained weldments, as shown in Fig. 2. Tensile test was then carried out using CSS-44100 universal testing machine with a 100 KN load cell and a crosshead speed of 3 mm/min. For each welding parameter, at least three tensile samples were examined and the average of the test results was adopted. After tensile test, fracture locations of samples were photographed for investigating the fracture behavior of the tensile samples. At last, facture surfaces were examined by using scanning electron microscope (SEM) to investigate the tensile behaviors in detail.

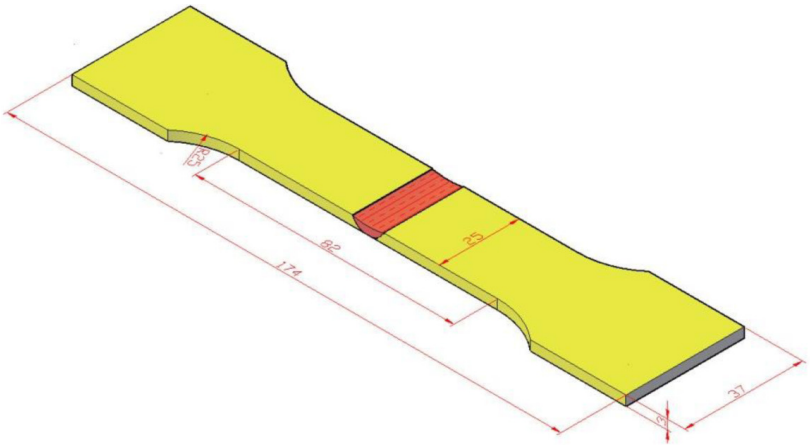

Figure 2. Drawings of tensile sample

3. Results and Discussion

3.1. Evolution of Microstructure and Precipitate

Figure 3 shows the cross-sections of the as-welded AZ80 FSW joints from all the welding parameters. The weld is universally consisting of nugget zone (NZ), thermo- mechanically affected zone (TMAZ), heat affect zone (HAZ), and base metal (BM). It is found in Fig. 3 that although sound welds could be obtained in most of the welding conditions, there are typical welding defects in some of the joints. Apparent welding defects found in this study are root defect and tunnel defect which form commonly at the root of NZ in AS and inner the weld. Similar results can also be found in Cao's FSW study on AZ31 alloy[6].

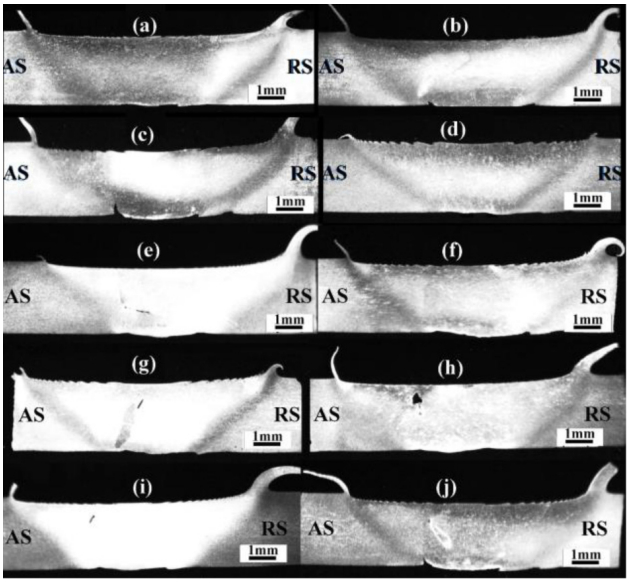

Figure 3. Cross-sections of the as-welded joints from the welding parameters of (a) 1000-80 (rotational speed in rpm – welding speed in mm/min), (b) 1000-150, (c) 1000-300, (d) 1000-400, (e) 1250-150, (f) 1250-300, (g) 1250-400, (h) 1500-150, (i) 1500-300, (j) 1500-400

The microstructures of different regions through the weld are shown in Fig. 4. Fig. 4a shows that the microstructure of the base material (BM) is uniform and boundaries between grains are not clear. As shown in Fig. 4b, the further SEM observation reveals that the microstructure involves several discontinuous precipitations (DP) and continuous precipitations (CP) named β-$Mg_{17}Al_{12}$ phases in α-Mg matrix and grain boundaries [1]. In NZ, as shown in Fig. 4c, the microstructure is of homogeneous fine equated grains with the characteristics of recrystallization. Fig. 4d&e reveal the microstructure of transition zone between TMAZ and NZ. It can be observed that recrystallization also occur in this region, but the grains are highly deformed and elongated. As shown in Fig. 4f, morphology of grains with incomplete recrystallization characteristics is found in HAZ.

SEM morphologies in different zones of the weld are shown in Fig. 5. They reveal that the precipitate distributions features in different regions would exhibit significant difference compare with the base metal. In NZ, as shown in Fig. 5b, most of the continuous and discontinuous β-$Mg_{17}Al_{12}$ precipitations in BM were disappeared after FSW. Fig. 5b also reveals that most of the recrystallized fine grains in NZ could be outlined with several precipitate particles. That indicates the β-$Mg_{17}Al_{12}$ phase in the base metal would dissolve into the Mg matrix, and the redistribute at the boundaries of equiaxed grains resulting in the formation of β phase net-work structure [17]. In TMAZ, as shown in Fig. 5c the features of microstructures and precipitation distributions are similar that in NZ where recrystallization and redistribution behavior are also performed. However, within HAZ where the microstructure of incomplete recrystallization is found, there are still some retained β phases with a continuation of the base metal.

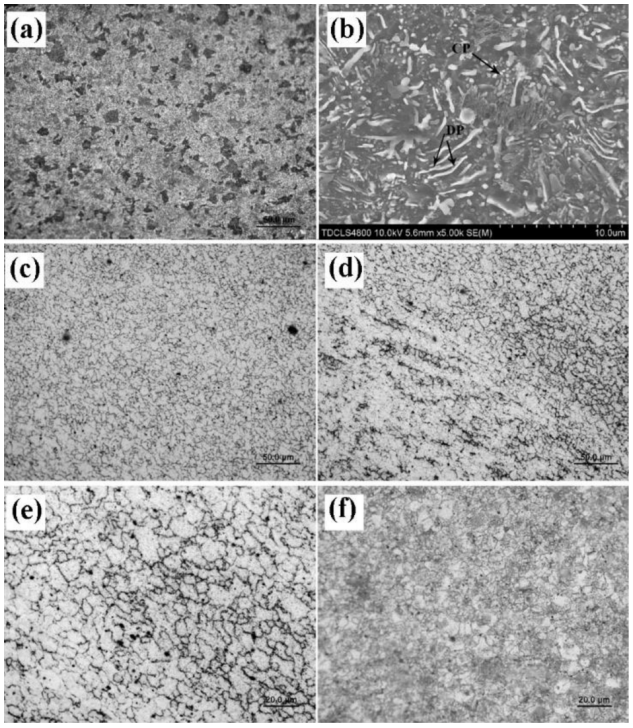

Figure 4. (a) and (b) OM and SEM image microstructure of the base material and OM images of microstructures of FSW AZ80 *joints*: (c) NZ, (d) transition zone, (e) TMAZ, and (f) HAZ

The X-ray diffraction patterns of different regions in the weld are shown in Fig. 6. In the base metal, beside several peaks of magnesium matrix with relatively high intensity, there are also some peaks indicating the existence of a large amount of β-$Mg_{17}Al_{12}$ phase. However, in NZ and TMAZ, as show in Fig. 6, most of β phase peaks are disappeared. Combining with the results from Fig. 5, it is believed that most of the intra-granular β precipitates in NZ and TMAZ would dissolve into the Mg matrix to form supersaturated solid solution owing to the plastic deformation and thermal process during FSW. In these two regions the precipitates redistribute around the grain boundaries which have been totally recrystallized in both FSW and cooling process. In HAZ, however, where incomplete recrystallization is found, most of the intra-granular DP particles were dissolved, but there are also some of the coarsening CP particles.

3.2. Mechanical Properties

Fig. 7 shows the hardness distribution features of AZ80 welds welded with 1000 rpm rotational speed and various welding speeds. From all the testing results, a uniformly V-like shape is found and no obvious variation low can be found when different the welding speed is used. Most of the lowest hardness values ranging from 55 $HV_{0.1}$ to 67 $HV_{0.1}$ are found at NZ with 4 mm width along the testing line on the weld. Going 2 mm ~ 5 mm far away from the weld

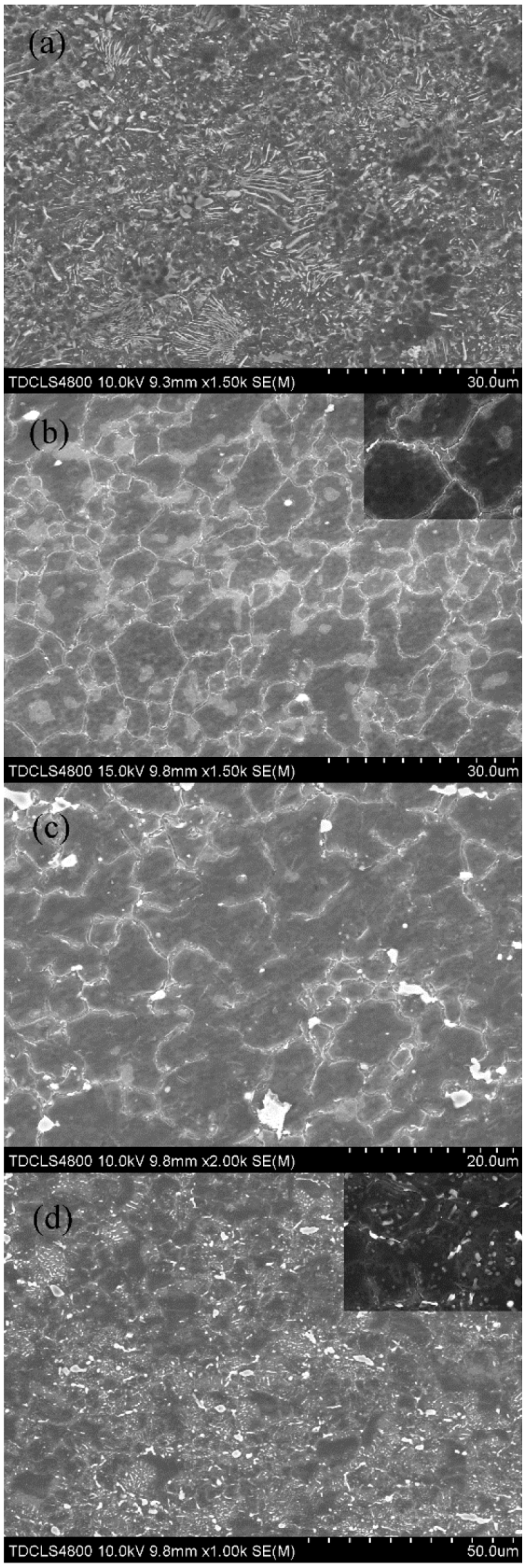

Figure 5. The SEM images of the microstructure of the weld in different regions (a) base metal, (b) nugget zone, (c) TMAZ, and (d) HAZ

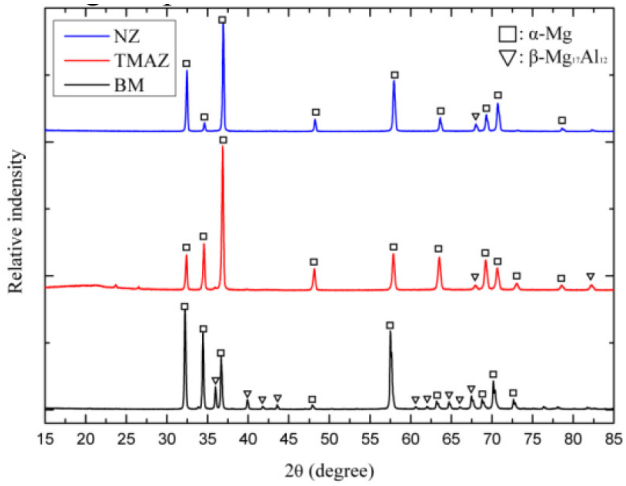

Figure 6. XRD patterns of the base metal, TMAZ and NZ of the welds

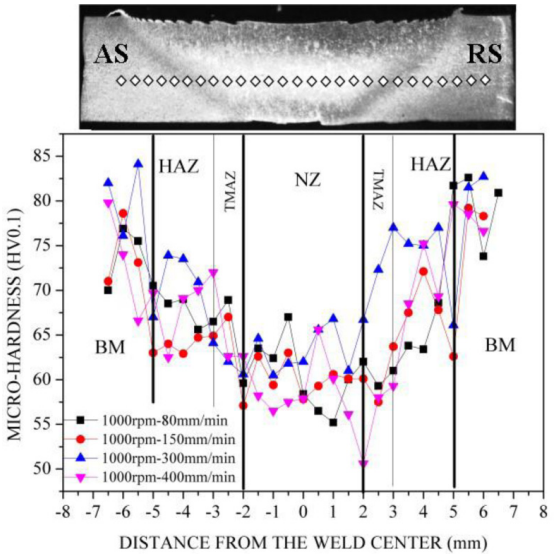

Figure 7. Micro-hardness of the joints at different welding parameters

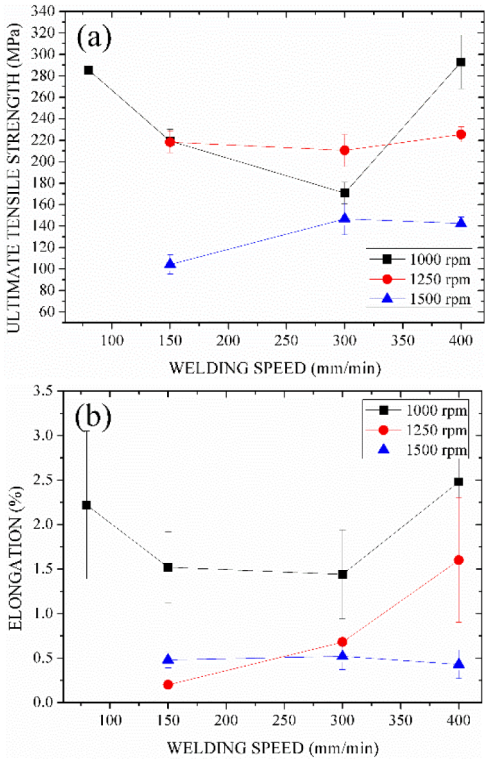

Figure 8. Tensile properties of FSW AZ80 welds: (a) ultimate tensile strength and (b) elongation of the welds in different welding conditions

center where TMAZ and HAZ are located, a significant increase of hardness values is obtained. Moreover, the hardness of TMAZ and HAZ in RS exhibit higher in value than that in AS.

The significant decrease of hardness in NZ, TMAZ, and HAZ might due to the solution behavior of strengthening phases in AZ80 alloy during FSW process. As is well known that the AZ80 alloy is a kind of age-hardening magnesium alloy by means of the direct transformation of equilibrium β-$Mg_{17}Al_{12}$ precipitates without any G.P zone or any intermediate phases [1]. The β-$Mg_{17}Al_{12}$ phase has a relatively low melting point of 462°C [17] which is much lower than the temperature where at least 90°C in HAZ could easily be obtained in FSW of Mg alloys [4]. According to the SEM observations and XRD patterns mentioned above, it can be concluded that most of the β precipitates in weld zone were dissolved into the Mg matrix to form supersaturated solid solutions and only a limited volume of β precipitates retained at grain boundaries. In such materials and welding conditions, the softening behavior of weld region is dominated by the disappearance of β precipitates. In addition, neither fine-grain strengthening or strain hardening can be found obviously in the present study.

Fig. 8 presents the tensile properties of the obtained AZ80 welds in the present study. It is found in Fig. 8a&b that the ultimate tensile strength (UTS) and elongation of the welds are ranged in 100~289 MPa and 0.2~2.6% respectively. Specimens from lower rotational speed of 1000 rpm exhibit better tensile properties, where the highest 289 MPa UTS and 2.6% elongation could be obtained. Increasing the rotational speed up to 1500 rpm leads to significantly decrease of tensile properties. As shown in Fig. 8a&b, the high rotational speed samples exhibit extremely poor mechanical properties of 100~140 MPa UTS and 0.3~0.5% elongation.

Table 1 summarizes the welding defects, joint efficiencies, and failure modes of the welds from all the welding conditions. It can be observed that tensile strength for all the welds are much lower than the base metal. However, in defect free joints welded with 1000 rpm the joint efficiency would around 0.8 of the base metal (samples 1 and 4 in Table 1). Observing the fracture samples in tensile test, totally

Table 1. Summary of tensile test result

No.	Rotational speed (rpm)	Welding speed (mm/min)	Defect examination	Joint efficiency	Failure modes
1	1000	80	--	0.79	HAZ (AS)
2	1000	150	root defect	0.61	TMAZ at root defect (AS)
3	1000	300	root defect	0.47	TMAZ at root defect (RS)
4	1000	400	--	0.81	TMAZ (AS)
5	1250	150	Tunnel	0.61	TMAZ (RS)
6	1250	300	--	0.58	TMAZ (RS)
7	1250	400	--	0.62	HAZ (AS)
8	1500	150	Tunnel	0.30	NZ
9	1500	300	--	0.41	NZ
10	1500	400	root defect	0.40	NZ at root defect(AS)

three failure locations of TMAZ, HAZ, and NZ refer to TMAZ, HAZ, and NZ fracture separately as shown in Fig. 9. It is found that the root defects would lead an obvious reduction for both UTS and elongation of the weld. That is mainly because cracking would more likely initiate at notch tip of the root defect and propagate into the weld regions under the tensile load. Moreover, the influence of tunnel defects on the joint tensile properties is found as rare in the present study.

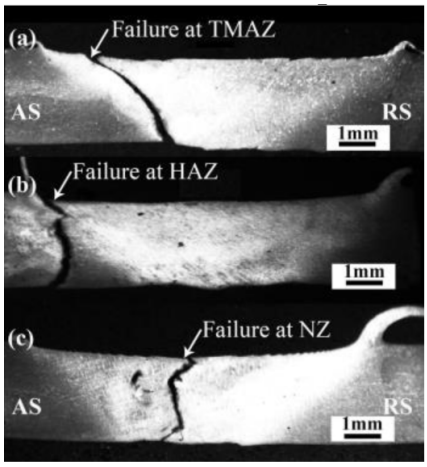

Figure 9. Typical fracture mode in tensile tests: the specimens failure at (a) TMAZ of 1000-400, (b) HAZ of 1000-80, and (c) NZ of 1500-300

The significant reduction of joints' tensile properties comparing with the base metal is also close related to the material softening behavior and the redistribution of equilibrium β-$Mg_{17}Al_{12}$ precipitates during the FSW process. As is illustrated in Fig. 7, hardness value of weld zone including NZ, TMAZ, and HAZ is much lower than that of the base metal. When the effect of welding defect is rare, yielding and plastic deformation of the material would occur more likely at softened regions. In previous sections, we also found that most of the strengthening precipitates of β-$Mg_{17}Al_{12}$ in weld zone were dissolved into the Mg matrix and redistributed at grain boundaries to form net-work microstructures in NZ, TMAZ, which would lead stress concentration at grain boundaries and further induce brittle fracture at low stress. This might be the major reason of the reduction in both strength and ductility of the weld.

3.3. Fracture Morphology

To explore the fracture behavior in much more details, typical fracture surfaces obtained in tensile experiment are examined by SEM observation. Fig. 10 shows the SEM morphology of the fracture surface of failure samples obtained in the present study. As shown in Fig. 10a, the fracture mechanism of BM belongs to quasi-cleavage fracture whose characteristics are of both ductile and brittle. It is revealed in Fig. 10b&c that the feature of samples fracture at TMAZ is also dominated of quasi-cleavage morphology of which some tear ridges and elongated cleavage plane could be found at the fracture surface. In Fig. 10d, it can be observed that, fracture surface with quasi-cleavage morphology could also be found in HAZ failure samples, unlike TMAZ fracture, however, the overall fracture surface has rare distinction of significant deformation and elongation of grains. Moreover, as shown in Fig. 10e&f, the samples fracture at both NZ and TMAZ under low stress and with poor elongations exhibit brittle features throughout the fracture surfaces.

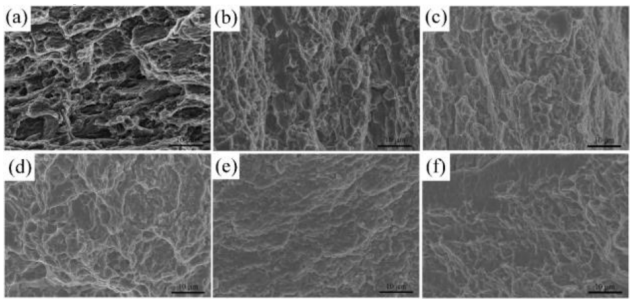

Figure 10. SEM images of fracture surfaces in tensile specimens from (a) the base metal, (b) Sample 1 fracture at HAZ, (c) Sample 3 with root defect fracture at TMAZ, (d) Sample 4 fracture at TMAZ , (e) Sample 5 fracture at TMAZ, and (f) Sample 10 with root defect fracture at NZ

Conclusions

In the present study, microstructures and mechanical properties of AZ80 magnesium alloy welds fabricated with friction stir welding (FSW) were systematically investigated. Main results can be concluded as follows:

Defect free welds could be obtained with the optimum parameter combinations of 1000 rpm rotational speed and welding speeds of 80 and 400 mm/min. At higher rotational speed ranging from 1250 to 1500 rpm, tunnel defects would form inner the weld. In some situations, notch like defects could also be found at the weld root.

The microstructure of NZ is consist of fine recrystallized grains. In TMAZ there are several highly deformed and elongated recrystallization grains. In HAZ, microstructures with features of incomplete recrystallization could be observed.

SEM and XRD investigations of NZ and TMAZ indicate that most of the β-$Mg_{17}Al_{12}$ precipitates of base metal would dissolve into the Mg matrix and could re-precipitate at grain boundaries. Dissolution and redistribution of precipitates leads the formation of net-work like microstructure which is adverse the weld mechanical properties.

Significant reduction of hardness is found in NZ, TMAZ, and HAZ owing to the disappearance of strengthening phases. The FSW AZ80 joints could have acceptable strength and plasticity of 289 MPa ultimate tensile strengths and 2.6% elongation respectively. Text (not necessarily in a form of numbered list)

Acknowledgements

The authors acknowledge the financial support for this work from the National Nature Science Foundation of China (No.50775159).

References

1. D. Zhao, Z. Wang , M. Zuo, H. Geng. Effects of heat treatment on microstructure and mechanical properties of extruded AZ80 magnesium alloy. Mater Design. 2014,56,p.p.589-593.
2. Q. Guo, H-g. Yan, Z-h. Chen, H. Zhang. Fracture behaviors of AZ80 magnesium alloy during multiple forging processes. T Nonferr Metal Soc. 2006,16,p.p.922-926.
3. J-f. Jiang J-f, Wang Y, Du Z-m, Luo S-j. Microstructure and properties of AZ80 alloy semisolid billets fabricated by new strain induced melt activated method. T Nonferr Metal Soc. 2012,22, Supplement 2,p.p.s422-s427.
4. Commin L, Dumont M, Masse JE, Barrallier L. Friction stir welding of AZ31 magnesium alloy rolled sheets,p.p. Influence of processing parameters. Acta Mater. 2009,57,p.p.326-334.
5. Cao X, Jahazi M, Immarigeon JP, Wallace W. A review of laser welding techniques for magnesium alloys. J Mater Process Tech. 2006,171,p.p.188-204.
6. Cao X, Jahazi M. Effect of welding speed on the quality of friction stir welded butt joints of a magnesium alloy. Mater Design. 2009,30,p.p.2033-2042.
7. Rose AR, Manisekar K, Balasubramanian V. Effect of axial force on microstructure and tensile properties of friction stir welded AZ61A magnesium alloy. T Nonferr Metal Soc. 2011,21,p.p.974-984.
8. Lee WB, Kim JW, Yeon YM, Jung SB. The joint characteristics of friction stir welded AZ91D magnesium alloy. Mater Trans. 2003,44,p.p.917-923.
9. Dobriyal RR, Dhindaw BK, Muthukumaran S, Mukherjee SK. Microstructure and properties of friction stir butt-welded AE42 magnesium alloy. Mat Sci Eng a-Struct. 2008,477,p.p.243-249.
10. Yu SR, Chen XJ, Huang ZQ, Liu YH. Microstructure and mechanical properties of friction stir welding of AZ31B magnesium alloy added with cerium. J Rare Earth. 2010,28,p.p.316-320.
11. Mishra RS, Ma ZY. Friction stir welding and processing. Mat Sci Eng R. 2005,50,p.p.1-78
12. Nandan R, DebRoy T, Bhadeshia HKDH. Recent advances in friction-stir welding - Process, weldment structure and properties. Prog Mater Sci. 2008,53,p.p.980-1023.
13. Ma ZY, Liu FC, Mishra RS. Superplastic deformation mechanism of an ultrafine-grained aluminum alloy produced by friction stir processing. Acta Mater. 2010,58,p.p.4693-4704.
14. Xie GM, Ma ZY, Geng L, Chen RS. Microstructural evolution and enhanced superplasticity in friction stir processed Mg-Zn-Y-Zr alloy. Journal of Materials Research. 2008,23,p.p.1207-1213
15. Park SHC, Sato YS, Kokawa H. Microstructural evolution and its effect on Hall-Petch relationship in friction stir welding of thixomolded Mg alloy AZ91D. J Mater Sci. 2003,38,p.p.4379-4383.
16. Cao X, Jahazi M. Effect of tool rotational speed and probe length on lap joint quality of

a friction stir welded magnesium alloy. Mater Design. 2011,32,p.p.1-11.
17. Wang Z, Yang Y, Li B, Zhang Y, Zhang Z. Effect of hot-deformation on microstructure and mechanical properties of AZ80 magnesium alloy. Materials Science and Engineering A. 2013,582,p.p.36-40.
18. Pareek M, Polar A, Rumiche F, Indacochea JE. Metallurgical evaluation of AZ31B-H24 magnesium alloy friction stir welds. J Mater Eng Perform. 2007,16,p.p.655-662.
19. Darras B M, Khraisheh M K, Abu-Farha FK, Omar MA. Friction stir processing of commercial AZ31 magnesium alloy. Journal of Materials Processing Technology. 2007,191,p.p.77-81.
20. G. Padmanaban, V. Balasubramanian. An experimental investigation on friction stir welding of AZ31B magnesium alloy. Int J Adv Manuf Tech. 2010,49,p.p.111-121.

3D Virtual Fabric Dynamic Simulation Based on Improved Spring-Mass Model

Yan Fanlei*, Yang Lianhe

Key Laboratory of Advanced Electrical Engineering and Energy Technology, Tianjin Polytechnic University, Tianjin 300387, China
School of Electrical Engineering and Automation, Tianjin Polytechnic University, Tianjin 300387, China
School of Computer Science and Software Engineering, Tianjin Polytechnic University, Tianjin 300387, China

Abstract
The dynamic simulation technology of virtual fabrics has a wide range of applications in e-commerce, garment CAD, digital games and other fields. By focusing on the dynamic simulation of 3D virtual fabrics, and taking full account of the internal and external forces received by fabrics, this paper has simplified the classic spring-mass model, omitted the bending spring, and merged the structural spring and shear spring into linked spring; full considerations are given to the properties of fabric materials during the calculation of stress, and some critical mechanics parameters are also estimated; furthermore, the "hyper elasticity" problem is solved through self-adaptive control of particle positions according to inverse order and in the light of particle stress size; numerical integration is conducted through the selection and use of Velocity-Verlet method; the experimental results show that the simulation has achieved good velocity and realist effects.
Keywords: VIRTUAL FABRICS, DYNAMIC SIMULATION, SPRING-MASS MODEL